ELSEVIER

Cement & Concrete Composites 23 (2001) 207–214

Cement & Concrete Composites

www.elsevier.com/locate/cemconcomp

# Recognition of clinker phases by automatic image analysis

Michel Jourlin *, Bernard Roux, René-Michel Faure

*Laboratoire Image, Signal et Acoustique, Ecole Supérieure de Chimie, Physique Electronique de Lyon, BP 2077, 43 Boulevard du 11 novembre 1918, 69616 Villeurbanne Cedex, France*

**Abstract**

Microscopical analysis of clinker phases provides useful informations about its structure and its manufacturing process. This paper deals with automatic segmentation of clinker phases images acquired on polished sections using optical microscopy. The main difficulty lies in the segmentation step. Even sophisticated techniques using textural characterization did not give satisfactory results. Indeed, the concerned textures show variations from an image to another and their spatial extent may vary as well. The most efficient methods we have developed combine automated thresholding algorithms and the use of contrast. This latter notion is defined within the scope of a mathematical model: the logarithmic image processing (LIP) model. Considering the limited reproductibility of the chemical etches used to bring the phases to the fore and the variations in terms of shape and hue of the elements to be segmented, the proposed algorithms have to be adapted to clinkers of various origin. However their efficiency has been proved for one type of clinker. 

**Résumé**

L' analyse microscopique des phases de clinker fournit des informations intéressantes sur sa structure et sur le procédé de fabrication. Cet article s'intéresse à la segmentation automatique des images de phases de clinker acquises en microscopie optique sur des sections polies. La difficulté principale est l'étape de segmentation. Même des techniques évoluées utilisant le concept de texture ne donnent pas de résultats satisfaisants. En effet, les textures concernées présentent des variations d'une image à l'autre et leur étendue spatiale peut varier aussi. Les méthodes les plus efficaces que nous ayons développées s'appuyent à la fois sur des algorithmes de seuillage automatique et sur la notion de contraste. Celle-ci est exploitée dans le cadre d'un modèle mathématique: le modèle logarithmic image processing (LIP). Compte tenu de la reproductibilité limitée des attaques chimiques utilisées pour mettre les phases en évidence et les variations en terme de teinte et de forme des éléments à segmenter, les algorithmes proposés doivent s'adapter à des clinkers de différentes origines. Cependant, leur efficacité a été prouvée pour un type de clinker. 

*Keywords:* Clinker; Image analysis; Segmentation; Thresholding; Contrast

## 1. Introduction

The clinker results from firing a raw mix made of limestone and clay principally. After the burning process, the clinker looks like granules more or less spherical that are crushed for giving cement. The microscopical examination of polished sections of cement clinkers brings a visual appreciation of crystal size, morphology, abundance and distribution (Fig. 1). Image analysis is rarely used to study the structure of clinker phases or cement, except in observing back-scattered electron images of polished sections, in connection with energy dispersive X-ray (EDX) detectors to produce atomic elements dot maps. In this case, the segmentation of phases becomes evident. Optical microscopy is more widespread and less costly but necessitates image analysis in order to separate phases. The microscopy permits a characterization of the clinker thin structure, of the minerals morphology and their distribution inside the clinker grains.

The present paper deals with optical microscopy and the associated image analysis. Such an approach aims at an objective quantitative evaluation of the clinker main constitutive phases, namely the alite $(SiO_2)$ $(CaO)_3$ denoted $C_3S$ in the cement industry, the belite $(SiO_2)$ $(CaO)_2$ denoted $C_2S$ (Figs. 2–5) and the matrix, union of the two aluminates $(Al_2O_3)$ $(CaO)_3$ denoted $C_3A$ and

* Corresponding author.

0958-9465/01/$ - see front matter 
PII: S0958-9465(00)00080-9

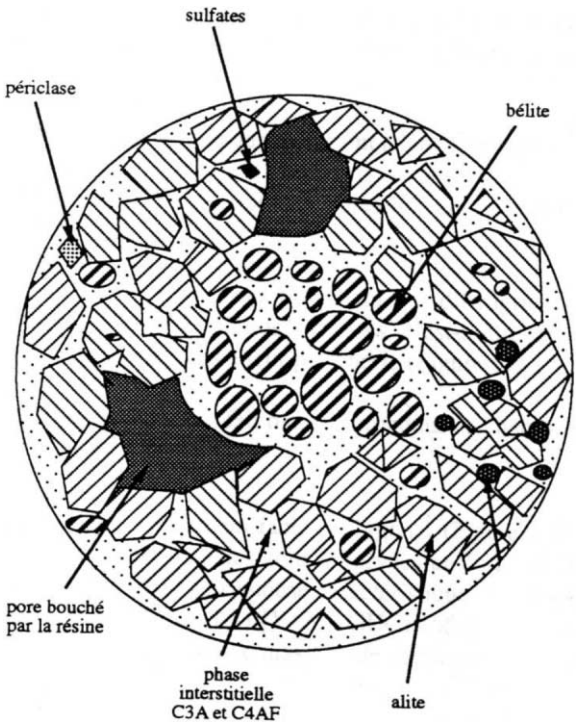


Fig. 1. Simplified representation of a clinker polished section.

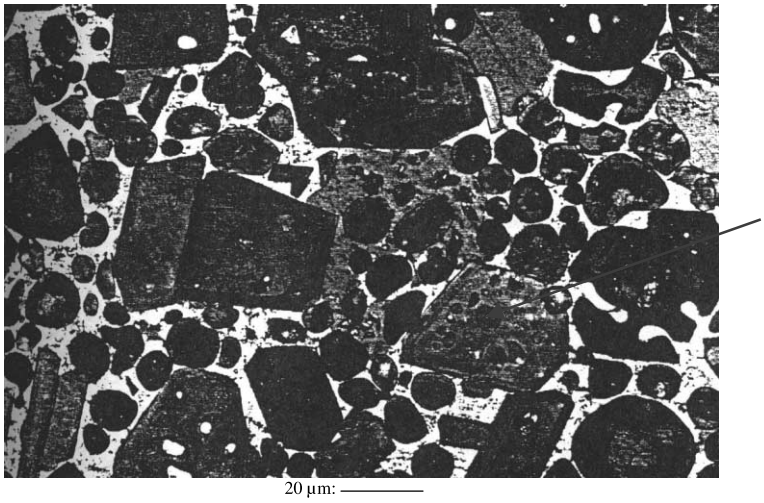


Fig. 2. Belite inclusions in alite, attack: $HNO_3 + NH_4Cl$.

$(Al_2O_3)$ $(Fe_2O_3)$ $(CaO)_4$ denoted $C_4AF$. Other secondary elements are present: free lime CaOL, magnesia MgO and sulphates.

On polished sections without chemical attack, alite crystals present a grey hue. After the attack, the contours are usually well contrasted. The inclusion of other minerals, belite in particular, is classical.

The normal size of alite elements lies between 25 and 65 μm.

On polished sections without attack, the belite grains present a darker aspect, their size is approximately 30 μm and their shape, rather ''rounded'', is variable: in fact, the crystals surface may be smooth, and more generally, it presents a double striation.

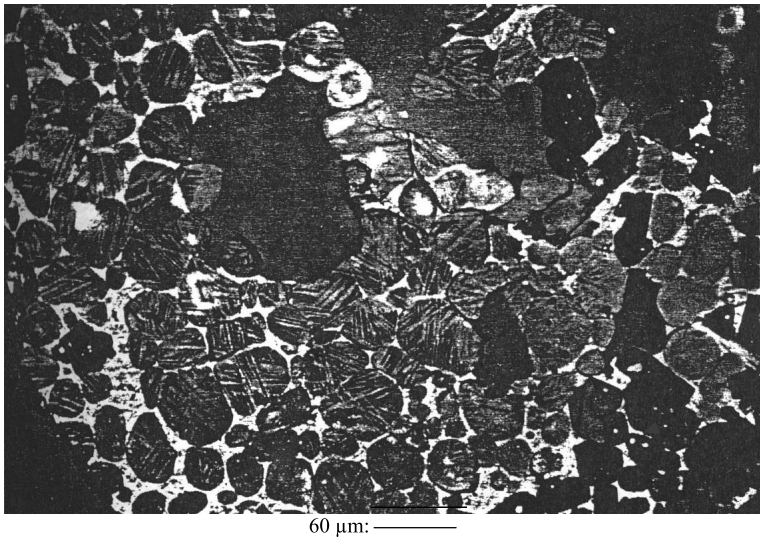


Fig. 3. Double striation on belite, borax attack.


Fig. 4. Belite rosette (clayey origin).

Belite is observable as isolated grains, or grains groups or ''rosettes''.

The variability of shape and aspect of the elements to be observed clearly makes difficult an automated image interpretation.

## 2. Images acquisition

The image acquisition system is illustrated in Fig. 6.

The black and white CCD sensor is fixed on the microscope equipped with a green-filter. The image resolution is $512 \times 512$ pixels and 256 grey levels.

The stage must be programmable in order to observe the successive fields and must be driven by an automated focusing algorithm such that all the acquired images are not blurred. The driving parameter selected for the focusing consists in maximizing the gradient integral: in fact, in the focusing plane, the grey level variations are not attenuated and are then maximal.

## 3. Image processing

The images to be processed may be classified into three different groups.

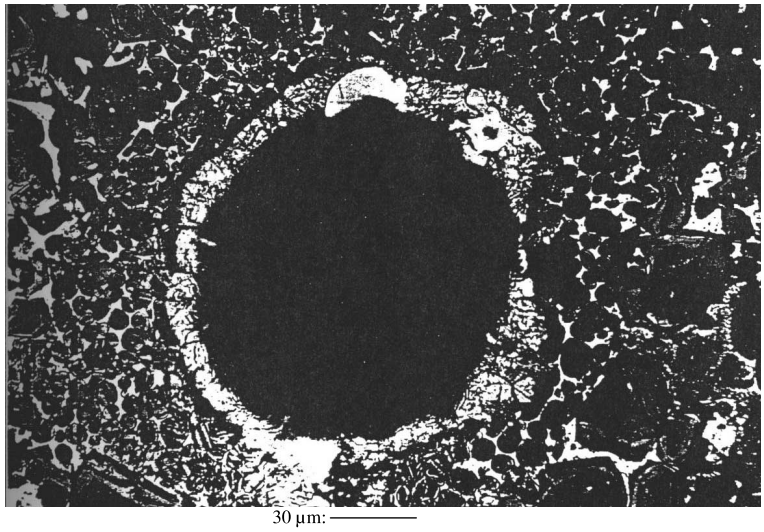


Fig. 5. Belite rosette (siliceous origin).

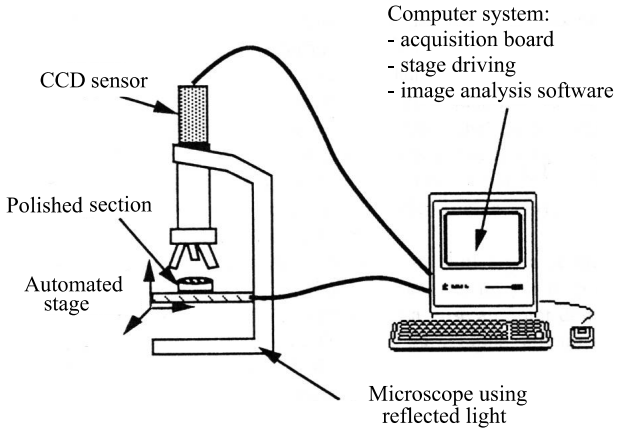


Fig. 6. Acquisition system.

*Group* I (Fig. 7). Images with a low magnification (fields larger than 1 mm in length) on polished sections without attack. Such images are used for the study of porosity and free-lime.

The pores are dark or medium-grey according to their filling percentage by the resin. The free-lime appears as small black grains. The grey levels associated with the bright part of the grey scale correspond to the other phases and are difficult to separate.

*Group* II (Fig. 8). Images used to evaluate the alite, the belite and the matrix. The selected magnification is medium (fields of about 300 µm in length) and it is necessary to attack the section with borax to reveal the phases.

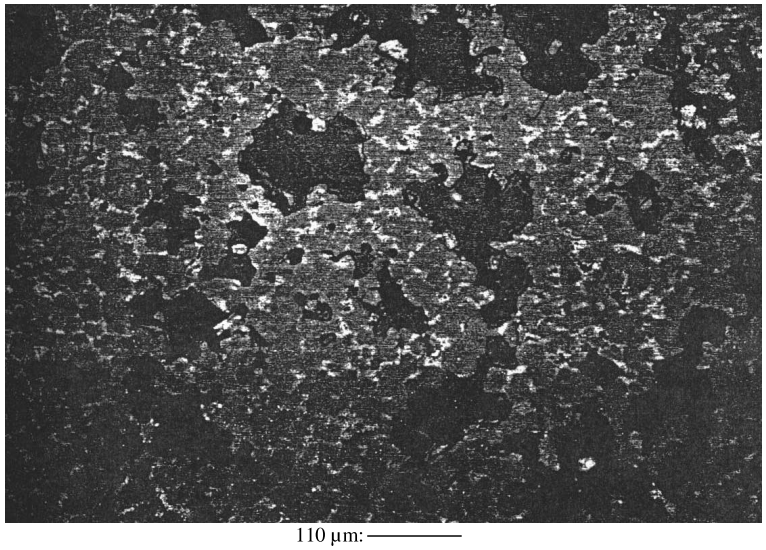


Fig. 7. Group I: clinker polished section without attack.


Fig. 8. Group II: clinker polished section with borax attack.

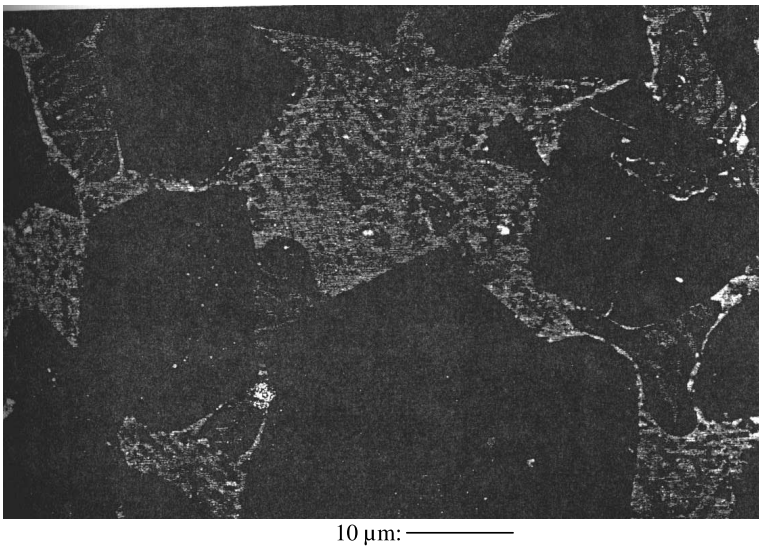


Fig. 9. Group III: clinker polished section.

*Group* III (Fig. 9). Images acquired under a high magnification (fields less than 100 μm in length) and for which the section has been attacked in order to reveal $C_3A$. Such images are used for individual analysis of $C_3A$ and $C_4AF$ and their overlapping.

A lot of segmentation methods related to the notion of texture or based on contour extraction of the grains have been tested without great success.

As a partial conclusion, we can consider that for Group II images, it is impossible to classify correctly the phases by means of a single process. Thus, the selected strategy is based on a sequence of processes.

The main steps may be described as follows:

(a) *Determination of the number of significant classes*. This evaluation is automatically performed using the notion of contrast associated with boundaries [1]. For each value of the threshold, the contrast of the boundary brought to the fore is computed: for each pair of neighbouring pixels separated by the threshold, the contrast is computed as their grey levels difference. Then the average contrast is evaluated on the set of all such pairs of neighbouring pixels. The contrast values associated with boundaries are presented as a histogram (Fig. 10). In this histogram, local maxima correspond to thresholds separating regions, except those which could be situated at the grey scale extremities. The number of representative classes corresponds to the number of these maxima plus one. In the case of the image under consideration, there are three classes.

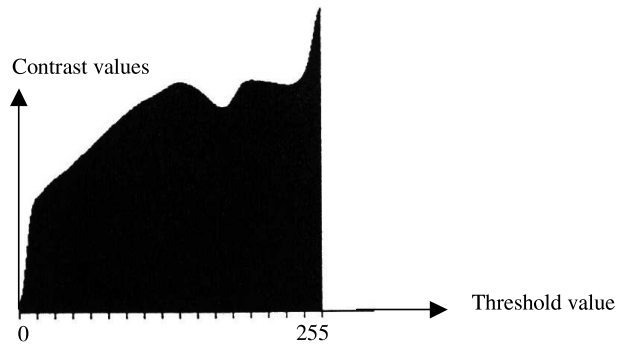


Fig. 10. Histogram of contrast values associated with boundaries.

Such an histogram is computed on all the pixels of the image.

(b) *Computation of contrast images*. The contrast is here intended in the sense of the LIP Model [cf. Appendix A]. In fact, this model has been proved to be well adapted to the human vision [2,3].

In a preprocessing step, the image is "normalized", in order to compensate lighting variations. That is to say, a certain coefficient $\lambda$ is computed in order that the LIP product of the grey level function $f$ by $\lambda : \lambda \otimes f$ corresponds to a mean grey level of 127 in the scale $[0, 255]$. Then the two contrast images associated, respectively, with the normalized image and its negative are computed. The grey level of each pixel is replaced by the contrast defined in formula (A.6) Appendix A.

(c) *Phases segmentation*. The two contrast images and the thresholds obtained by the technique presented in part (a) are used in order to classify the main phases: alite, belite and matrix. The flowchart of the image analysis steps is given in Fig. 11.

Some operations described hereupon necessitate complementary explanations:

(1) The binarization of the initial image displays bright regions corresponding to belite and matrix.

(2) The closing of the initial grey tone function is performed by means of an $11 \times 11$ square [4]: then, the difference between the closing and the initial image is computed and thresholded in order to obtain $C_3A$. Note that this difference operation is well known as the "Top-Hat Transform" introduced by F. Meyer [5].

(3) The metric thresholding approximates in an "optimal" way, the grey tone function by a step function [6]. The optimization is driven by a classical metric between functions, for example the volume between the two representative surfaces: when this distance is minimal, the step function is selected. This method, applied to the difference between the two contrast functions, displays the matrix.

(4) The first step of alite classification is the thresholding of the contrast image associated with the negative normalized image.

(5) Mathematical morphology [4,7] is used for cleaning images. Small objects are removed by a reconstruction after erosion.

## 4. Results

The original image in Fig. 12 has been processed in order to illustrate the pertinence of our approach in obtaining: alite, belite and matrix.

## 5. Conclusion

The presented algorithm generally gives satisfying results. Nevertheless, the method should not be considered as fully automated, due to the limited reproductibility of the chemical etch used to bring the phases to the fore and to the variations in characteristics (shape, hue, size) of the elements to be segmented. This method must be adapted to clinkers from different origins.

In all the tested situations, the matrix is well classified. In the case of free lime presence, it is usually segmented with alite, and some bright pores are displayed as belite.

## Appendix A. The LIP model

### *A.1. The LIP (logarithmic image processing) model and contrast*

Images obtained in transmitted light or those produced by the human visual system are logarithmic images. The LIP model [8] has been introduced to process these kinds of images. Images obtained in reflected light can, to a certain extent, fall within the scope of this model by replacing transmittance by reflectance.

A grey tone function can be associated with each image. It is defined on a compact set $D$ of the plane, called the spatial support, with a range of values in the real interval $[0, M[$. The value of $M$ is strictly positive and corresponds with the number of grey levels. The space of grey tone functions is called $G$. The sum of two images is defined by

$$f \boxplus g = f + g - \frac{fg}{M} \quad \forall (f, g) \in G^2. \tag{A.1}$$

The positive homothetic of an image is defined in the following way:

$$\alpha \otimes f = M - M\left[1 - \frac{f}{M}\right]^{\alpha} \quad \forall f \in G \quad \forall \alpha \in \Re. \tag{A.2}$$

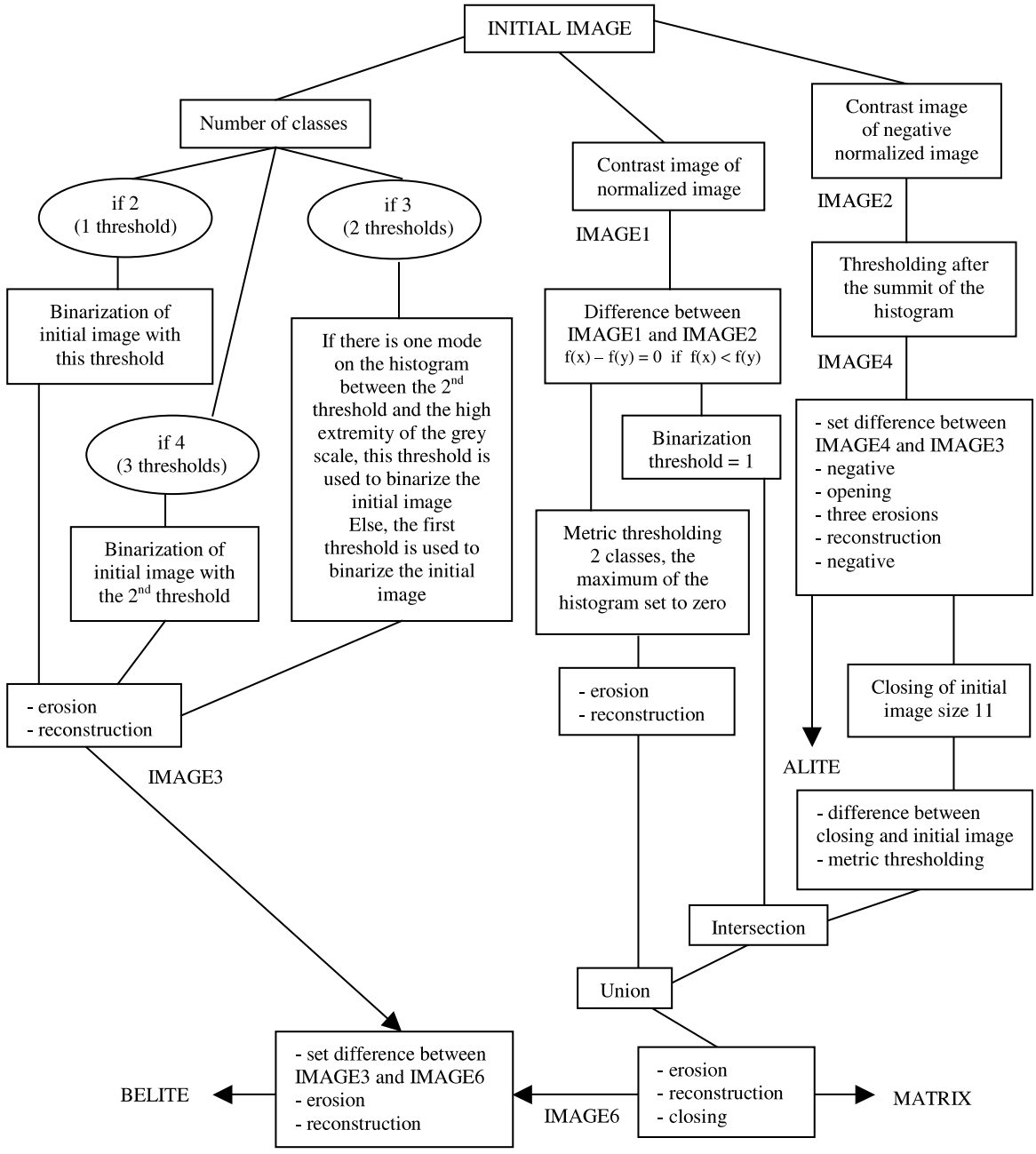


Fig. 11. Flowchart of the algorithm.

N.B.: Operators $\triangle$ and $\overline{\triangle}$ act on images while +, − and × act upon the underlying functions. One deduces the subtractive law:

$$f \overline{\triangle} g = \frac{M[f-g]}{M-g} \quad \forall (f,g) \in G^2. \tag{A.3}$$

*A.2. Contrast between two points [9]*

For an image $f$, the contrast between two arbitrary points $x$ and $y$ of $D$ is defined by:

$$C_{(x,y)}(f) = \frac{1}{\mathrm{d}(x,y)} \overline{\triangle} [\mathrm{Max}(f(x),f(y)) \overline{\triangle} \mathrm{Min}(f(x),f(y))] \quad \forall f \in G. \tag{A.4}$$

Or under another form:

$$C_{(x,y)}(f) = \frac{1}{\mathrm{d}(x,y)} \overline{\triangle} \frac{|f(x)-f(y)|}{1-\mathrm{Min}[f(x),f(y)]/M}, \tag{A.5}$$

where $\mathrm{d}(x,y)$ is the Euclidean distance between $x$ and $y$.

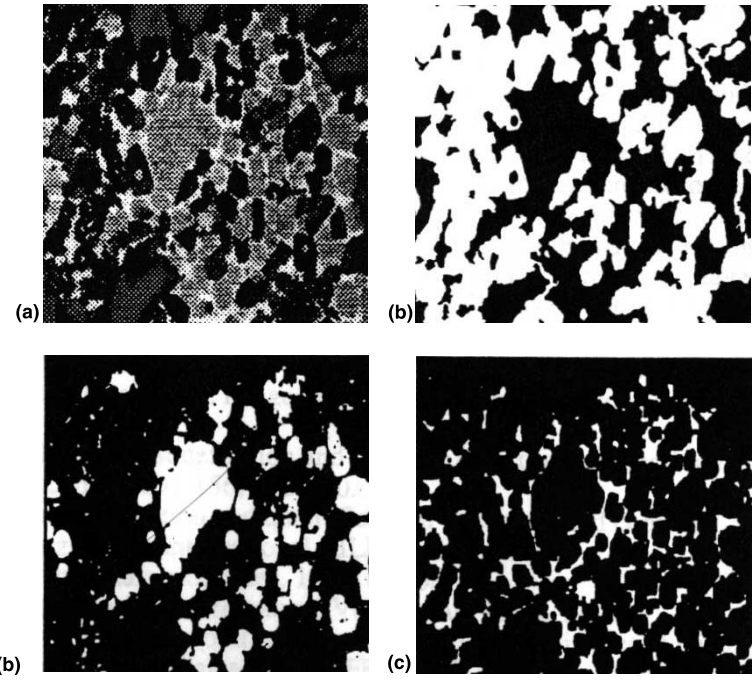


Fig. 12. (a) Original image. (b) Alite binary image. (c) Belite binary image. (d) Matrix binary image.

### *A.3. Contrast at a point*

Let $x_i$ be a neighbour of a pixel $x$ of $D$ and $n$ the number of neighbours taken into account ($n = 8$ in our application), the contrast at $x$ is defined by:

$$C_x(f) = \frac{1}{n} \bigtriangleup \bigtriangleup_{i=1}^{n} C_{(x,x_i)}(f). \tag{A.6}$$

### *A.4. Contrast associated with a boundary*

Considering a boundary $F$ separating two or several adjacent regions, the contrast associated with $F$ is given by:

$$C_F(f) = \frac{1}{\neq V} \bigtriangleup \bigtriangleup_{(x,y)\in V} C_{(x,y)}(f), \tag{A.7}$$

where $V$ represents the set of pairs of pixels separated by $F$ and $\neq V$ is the cardinal of $V$.

## References

[1] Zeboudj R. Du prétraitement à l'analyse d'image. Thèse de Doctorat de l'Université de Saint-Etienne; 1988.
[2] Pinoli JC. J Math Imag Vision 1997;7.
[3] Brailean JC, Sullivan BJ, Chen CT, Giger MI. Proc ICASSP 1991:2957.
[4] Serra J. Image analysis and mathematical morphology. London: Academic Press; 1982.
[5] Meyer F. Thèse de Docteur Ingénieur de l'Ecole Nationale des Mines de Paris; 1979.
[6] Labouré M.J., Faisabilité d'une carte électronique d'opérateurs de seuillage. Thèse de Doctorat de l'Université de Saint-Etienne; 1987.
[7] Coster M, Chermant JL. Précis d'Analyse d'Image. Presses du CNRS; 1989.
[8] Jourlin M, Pinoli JC. J Microsc 1988:149.
[9] Jourlin M, Pinoli JC, Zeboudj R. J Microsc 1989:156.